Eur. Phys. J. B **12**, 147–155 (1999)

THE EUROPEAN PHYSICAL JOURNAL B

EDP Sciences

CuCl nanocrystals in alkali-halide matrices under hydrostatic pressure

M. Haselhoff[a], K. Reimann[b], and H.-J. Weber

Institut für Physik, Universität Dortmund, 44221 Dortmund, Germany

Received 4 March 1999

Abstract. CuCl nanocrystals in crystalline alkali-halide matrices have been investigated under hydrostatic pressures up to 18 GPa. The pressures of structural phase transitions in CuCl have been determined both for different nanocrystal sizes and for different matrices (NaCl, LiCl, KCl). For CuCl nanocrystals in NaCl an increase of the transition pressure with decreasing nanocrystal size is observed, which is explained by the increasing importance of surface pressure for small nanocrystals. We found higher transition pressures for the LiCl matrix than for the NaCl matrix. The reason for this is that the pressure which acts on the nanocrystal differs from the external pressure. A simple elastic model describes the effective pressure transmitted from the matrix to the nanocrystal. With CuCl nanocrystals embedded in KCl we have studied the behavior of nanocrystals during a phase transition of the matrix. Additionally we have determined the pressure coefficients of the exciton energies of the CuCl nanocrystals, which depend on the elastic properties of the matrix.

PACS. 64.70.Kb Solid-solid transitions – 62.50.+p High-pressure and shock-wave effects in solids and liquids – 78.55.Hx Other solid inorganic materials – 71.35.Cc Intrinsic properties of excitons; optical absorption spectra

1 Introduction

Reducing the dimensionality from bulk over two-dimensional quantum wells and one-dimensional quantum wires to zero-dimensional quantum dots is an ongoing trend in semiconductor physics and technology (*cf.* the proceedings of the last ICPS conferences [1–3]). The emphasis is usually on the electronic properties of these semiconductor structures. Recently, however, there has developed interest also in the thermodynamic properties of nanometer-size particles, such as the size dependence of pressures for structural phase transitions in CdSe and CdS_xSe_{1-x} nanocrystals [4–6].

Obviously, the surface becomes more and more important when decreasing the particle size. For small enough particles surface tension leads to an important contribution to the Gibbs free energy, which determines the stable phase for a given pressure and a given temperature. Because of this the temperatures and pressures for phase transitions depend on the particle size.

From basic thermodynamics a decrease of phase transition temperatures and an increase of phase transition pressures is expected in the case of liquid droplets surrounded by vapor. In that case the surface tension is always positive. In principle, the concept of surface tension works also for solids, but in contrast to liquids the surface tension of crystals is anisotropic. Thus the equilibrium shape of a crystal is determined by the surface tensions of the crystal faces, as described by Wulff's relations [7]. For nanocrystals in a solid matrix an effective surface tension has to be considered, which also contains the interaction between nanocrystal and matrix. In this case the effective surface tension can have either sign, so that it is not *a priori* clear whether the transition pressure increases or decreases upon decreasing the nanocrystal size.

The interaction between the nanocrystal and the crystalline matrix depends on the orientation of the nanocrystals relative to the matrix. For the case of CuCl nanocrystals in a NaCl matrix this orientation was determined by two-photon absorption [8]. It was found that the crystalline axes of the nanocrystals are oriented parallel to the axes of the NaCl matrix. This orientation can be explained by an undisturbed lattice of the chloride ions in the crystal, whereas the alkali and copper ions change sites by diffusion during the growth process [9].

Bulk CuCl shows several pressure-induced structural phase transitions [10–16]. At $P = 5$ GPa there is a phase transition from the (ambient pressure) zinc-blende structure to an intermediate tetragonal structure, and above 10 GPa a second one to the sodium-chloride structure.

[a] e-mail: haselhoff@fkp.physik.uni-dortmund.de

[b] *Present address:* Max-Born-Institut für Nichtlineare Optik und Kurzzeitspektroskopie, Rudower Chaussee 6, 12489 Berlin, Germany.

These phase transitions can be detected optically, since the high-pressure phases are still semiconducting, but have different band gaps [14]. We have studied these structural phase transitions in CuCl nanocrystals of different sizes and in different alkali halide matrices (NaCl, KCl, and LiCl, see Sect. 3.1). Whereas for LiCl and NaCl the sodium chloride structure is stable in the pressure range investigated (up to 18 GPa), KCl has a phase transition from the sodium-chloride to the cesium-chloride structure. The effect of this phase transition of the matrix on the nanocrystals was investigated.

Apart from structural phase transitions we have also investigated pressure shifts of intrinsic transitions in the zinc blende phase of CuCl (Sect. 3.2). The pressure coefficients are found to depend on the matrix, since the pressure exerted on the nanocrystal in a crystalline matrix is not necessarily equal to the pressure applied from outside (Sect. 4).

2 Experiment

2.1 Sample preparation

NaCl, LiCl, and KCl single crystals doped with CuCl were grown by the Czochralski method. The Cu^+ concentration in the melt was about 3 mole% for LiCl and KCl and 1 mole% for NaCl. The CuCl concentration in the grown crystal, however, is much smaller, less than 0.1 mole%. Some experiments were performed on Bridgman-grown crystals, which have a higher CuCl content, but their crystal quality is worse.

The investigation of the size dependence of the phase transition in CuCl nanocrystals was performed in a NaCl matrix. For these experiments the copper-doped NaCl crystal was cleaved into several samples. Each sample was exposed to a special heat treatment to achieve nanocrystals of a certain size. The heat treatment starts with dissolving nanocrystalline CuCl, which may have developed during Czochralski growth, at a temperature of $T = 700$ K. The growth of nanocrystals then occurs at growth temperatures $T_{\rm gr}$ between 300 and 400 K. The samples were kept about three weeks at $T_{\rm gr}$ and then stored below 270 K to prevent further growth. A detailed description of the growth behavior of CuCl nanocrystals in alkali halides is given in [9,17].

Absorption spectra of some of these samples taken at $T = 78$ K are shown in Figure 1. One can clearly see that the exciton peaks are shifted towards higher energies compared to bulk CuCl (the Z_3 exciton in bulk CuCl is at 3.22 eV at this temperature), especially for the samples with low growth temperatures. Since the reason for this shift is the exciton confinement, one can use it to determine the mean radius of the nanocrystals. The confinement energy ΔE for the weak confinement regime was calculated by Ekimov and Éfros for spherical nanocrystals with radius r as [18]:

$$\Delta E = \frac{\hbar^2}{2M}\frac{\pi^2}{r^2}, \qquad (1)$$

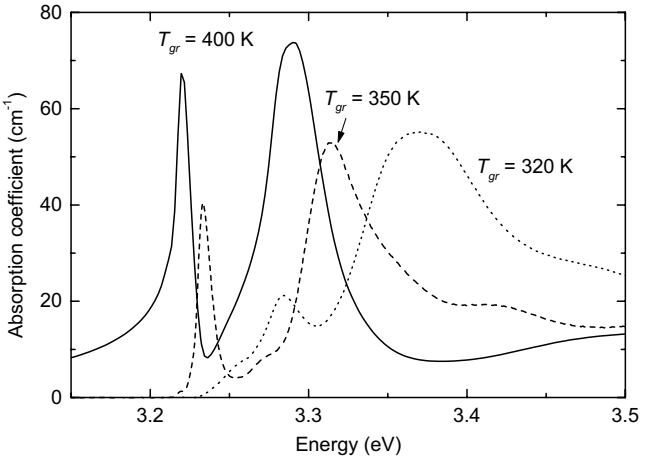

Fig. 1. Absorption spectra of CuCl nanocrystals in NaCl at $T = 78$ K after different heat treatments. The growth temperatures $T_{\rm gr}$ are given in the figure. The low energy peak is the Z_3 exciton and the high energy peak the $Z_{1,2}$ exciton of CuCl.

Table 1. Growth temperatures $T_{\rm gr}$, mean radii r of the CuCl nanocrystals, and the width $\Gamma_{3/4}$ (full width at three quarters of the maximum) of the Z_3 exciton for the samples used.

Matrix	NaCl				KCl	LiCl
$T_{\rm gr}$ (K)	300	320	350	400	300	–
r (nm)	1.5	1.6	3.3	10	2.6	> 10
$\Gamma_{3/4}$ (meV)	25	23	6	5		

with $M = 2.3\ m_0$ [19] for the total mass of the exciton. The mean radii obtained from the absorption spectra using equation (1) are given in Table 1. The width $\Gamma_{3/4}$ in Table 1, which is the full width at three quarters of the maximum, can be used as a measure of the size distribution. It should be noticed, that the increase of the confinement energy with decreasing nanocrystal size has to be considered for the interpretation of the linewidth.

The heat treatment of the CuCl:KCl sample consisted of dissolving the nanocrystals at $T = 600$ K and nanocrystal growth at room temperature for about 18 months. The absorption spectrum was measured from time to time at $T = 78$ K to determine the nanocrystal size. At the time of the experiments presented here the mean radius was 2.6 nm.

The CuCl:LiCl sample stems from an as grown crystal, which was kept below 270 K until the experiment. The mean nanocrystal radius in this sample was larger than 10 nm.

2.2 Optical techniques

Because of the very small CuCl contents of our samples and because of the small amount of material that can be used in diamond-anvil cells a determination of phase transitions by diffraction techniques is difficult or even impossible. Therefore we have performed photoluminescence

measurements. The phase transition is detected by the disappearance of peaks of the first phase and the appearance of new peaks. These measurements were done at low temperatures ($T = 7$ K) with the diamond anvil cell in a helium-flow cryostat. Low temperatures are needed for high luminescence efficiency and to prevent broadening of the peaks. For excitation of the luminescence we have used the UV line ($\lambda = 325$ nm) of a HeCd laser. The blue line ($\lambda = 442$ nm) of the same laser was used for excitation of the luminescence of ruby crystals, which were added to the sample for pressure determination. For the detection of the luminescence we have used a 0.85-m-focal-length double-grating spectrometer, a GaAs photomultiplier, and photon-counting electronics.

The pressure dependence of the band-structure of the Cu^+-doped NaCl crystal was investigated *via* absorption measurements. These measurements allow a direct determination of the confinement energy and of the pressure coefficients of the Z_3 and the $Z_{1,2}$ excitons of CuCl. The investigation of the LiCl sample was more complicated because it has a very high absorption. Therefore we have used for this sample luminescence excitation and two-photon absorption. For two-photon absorption a tunable dye laser pumped by the second harmonic of a pulsed Nd:YAG laser was used, for luminescence excitation the second harmonic of the same dye laser.

2.3 Pressure generation

High pressure was generated with a gasketed diamond-anvil cell (DAC), similar to the one described in [20], but smaller in dimensions. For pressure determination we have used the ruby luminescence scale [21,22].

To obtain homogeneous hydrostatic pressure, one has to use a fluid (gas or liquid) as pressure medium. Such a medium, however, does not exist at low temperatures. Even helium becomes solid at pressures above 0.03 GPa [23]. Nevertheless, helium generates the best hydrostatic conditions at low temperatures [24,25], provided the DAC is heated above the melting point of helium at the given pressure and cooled down after the pressure has been changed. Such a temperature cycling, however, is not applicable for the investigation of phase transitions, since it makes it difficult to separate the effects of temperature and pressure. A further problem is that the pressure inside the DAC changes during heating and cooling. Thus, the measurements have to be performed at constant temperature. Under such conditions helium does not give better hydrostatic conditions than alkali halides. Therefore we did not use an additional pressure medium, but simply filled the gasket hole with the sample and some ruby. In this way the matrix material itself acts as pressure medium. In the case of LiCl we have used *n*-heptane as pressure medium. Since LiCl is very hygroscopic *n*-heptane protects the sample at the same time from the water in the air when the sample is mounted into the DAC.

In Figure 2 we show the R_1 luminescence of ruby with NaCl as pressure medium at a temperature of 7 K and at a pressure of about 2.5 GPa. Since in this pressure range

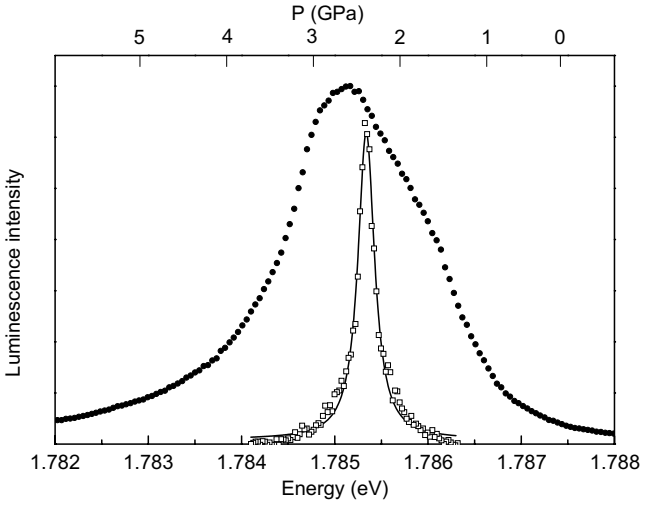

Fig. 2. Ruby luminescence at a temperature of 7 K for helium (open squares) and NaCl (closed circles) as pressure media at a pressure of about 2.5 GPa. The spectrum for helium has been fitted with a Lorentzian (solid line).

the pressure shift is nearly linear [22], the width of this line is proportional to the width of the pressure distribution in the DAC (see upper scale). The width of the pressure distribution obtained in this way is used in the analysis of our data on phase transitions (see Sect. 3.1). For comparison, we have also included in Figure 2 a R_1 spectrum obtained with helium as pressure medium after temperature cycling under otherwise similar conditions. The line width here is much smaller (and accordingly the pressure distribution much narrower). Therefore we have used helium as pressure medium in the determination of exciton pressure coefficients (Sect. 3.2), since for these measurements it was possible to do temperature cycling. Again LiCl was an exception because of its hygroscopicity.

3 Experimental results

3.1 Pressure-induced phase transitions

Here we present the investigation of pressure-induced phase transitions of CuCl nanocrystals in different alkali halides by photoluminescence measurements. To separate the luminescence of optical elements, of diamond anvils, and of the matrix (the background) from the luminescence of the nanocrystals, we have first measured the pressure dependence of the luminescence when the DAC was loaded with pure NaCl (the same material used for growing the crystals). The observed background is mainly caused by defects in NaCl [26]. It has a negligible pressure dependence.

As a next step we have measured the luminescence of bulk CuCl (grains of macroscopic dimensions) with NaCl as pressure medium up to $P = 16$ GPa (Figure 3) to be able to determine the phase transitions of the bulk material at low temperatures. At low pressures the spectra

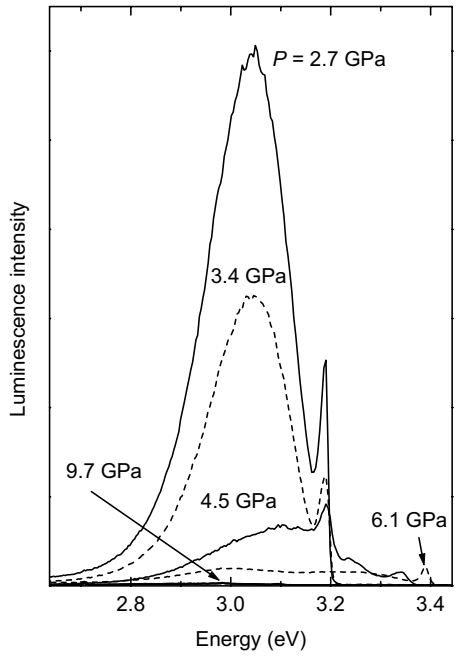

Fig. 3. Luminescence spectra of bulk CuCl with NaCl as pressure medium at a temperature of 7 K for different pressures.

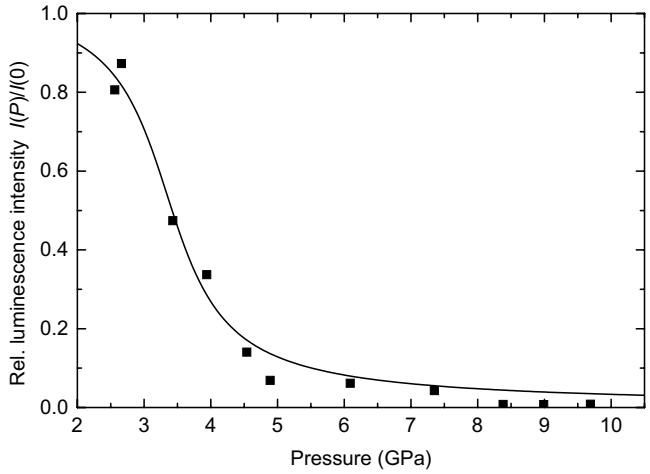

Fig. 4. Pressure dependence of the total luminescence intensity of bulk CuCl. The solid line is a fit assuming a pressure-independent width of the pressure distribution. The only fit parameter is the phase-transition pressure P_T.

consist of a sharp peak around 3.2 eV, which is caused by emission from the Z_3 exciton of CuCl, and of an impurity-induced broad band on the low-energy side. Both features are due to the zinc-blende phase of CuCl. At higher pressures one finds a blue shift of the lines (see Sect. 3.2) and an overall decrease of the intensity. This decrease is caused by the phase transition from the zinc-blende to the first high-pressure structure [14].

The pressure dependence of the total luminescence intensity is presented in Figure 4. For a first-order phase transition one would expect a step-like dependence of the intensity on pressure, i.e., a constant intensity below the phase transition pressure P_T and zero intensity above this pressure. Because of the pressure distribution in the DAC, which can be inferred from the ruby luminescence spectra (Sect. 2.3), this step-like behavior is smeared out. From the data we obtain a phase transition pressure of $P_T = 3.5$ GPa for bulk CuCl at $T = 7$ K.

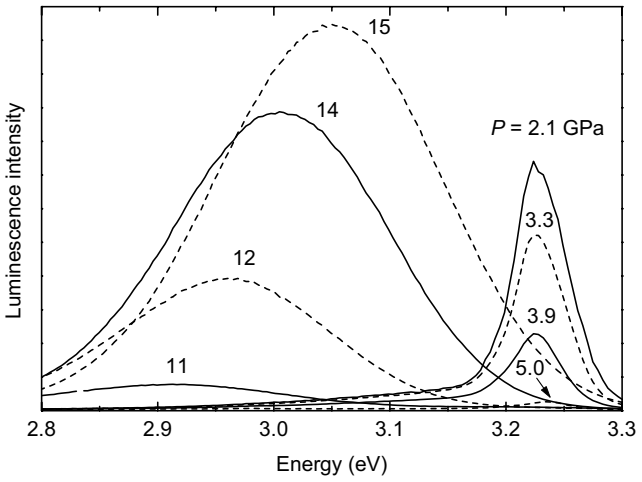

Fig. 5. Luminescence spectra of CuCl nanocrystals in NaCl (sample with $T_{gr} = 350$ K) for different pressures.

3.1.1 CuCl nanocrystals in NaCl

For CuCl nanocrystals in NaCl we have investigated the dependence of the phase-transition pressure on the nanocrystal size. Samples with different mean radii of the nanocrystals were prepared by annealing at different growth temperatures T_{gr} (see Sect. 2.1). As an example, we present in Figure 5 some luminescence spectra at different pressures of the sample with $T_{gr} = 350$ K measured at $T = 7$ K. Up to a pressure of 5.5 GPa the spectra consist of one peak around 3.23 eV, which decreases in intensity with increasing pressure. For pressures above 9.6 GPa a second peak occurs around 2.9 eV, which shows a blue-shift and an increase in intensity with increasing pressure. In the intermediate pressure range no luminescence from CuCl is observed. The peak at 3.23 eV stems from nanocrystals in the zinc-blende phase, whereas the low-energy peak is caused by CuCl in the sodium-chloride structure. We were not able to observe any luminescence from the intermediate phase, which corresponds to the observation in [27] that the luminescence from this phase is very weak.

The intensity of the zinc-blende luminescence is shown in Figure 6 as a function of pressure for the sample with $T_{gr} = 300$ K (small nanocrystals, $r = 1.5$ nm) and for the sample with $T_{gr} = 350$ K (medium nanocrystals, $r = 3.3$ nm). Whereas the data for the sample with $T_{gr} = 350$ K are very similar to the data of bulk CuCl, the sample with small nanocrystals shows the zinc-blende luminescence for a much wider pressure range. Thus, the phase transition for small nanocrystals occurs

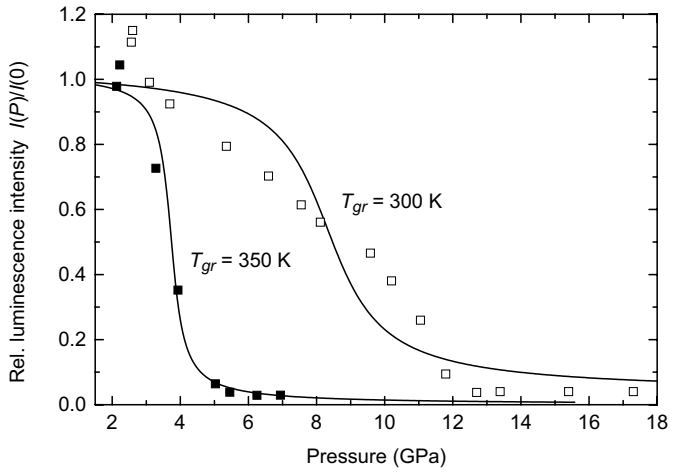

Fig. 6. Pressure dependence of the zinc-blende luminescence of CuCl nanocrystals in NaCl for the samples with $T_{\rm gr} = 300$ K ($r = 1.5$ nm) and $T_{\rm gr} = 350$ K ($r = 3.3$ nm). The solid lines are fits assuming a pressure-independent (for $T_{\rm gr} = 350$ K) or linearly increasing (for $T_{\rm gr} = 300$ K) width of the pressure distribution.

at considerably higher pressures than for larger nanocrystals or for bulk CuCl.

In contrast to the first phase transition from the zinc-blende structure to the intermediate phase the second phase transition to the sodium-chloride structure is found to be independent of the initial nanocrystal size. In all cases emission from the sodium-chloride phase begins at a pressure of about 10 GPa and the phase transition pressure is about 15 GPa.

The size dependence of the phase transition pressure from the zinc-blende structure to the intermediate phase is shown in Figure 7. For large nanocrystals one finds within experimental error the same value as for bulk CuCl, whereas P_T increases strongly for nanocrystals with radii less than 2 nm. This behavior is caused by the increasing amount of surface energy for small nanocrystals, as discussed in Section 4.

To clarify the influence of the matrix on structural phase transitions in CuCl, we have also investigated LiCl and KCl as matrices.

3.1.2 CuCl nanocrystals in LiCl

Since the CuCl nanocrystals in the LiCl sample are rather large, one expects the phase transition to occur at the same pressure as for bulk CuCl. Our experimental result, however, clearly shows that the phase transition occurs at a higher pressure than in bulk CuCl or in large CuCl nanocrystals in NaCl, namely at $P_T = 4.2$ GPa. Because of the large nanocrystal radius in this sample the reason for the pressure increase cannot be a surface effect. Instead this increase is due to the effect that the pressure acting on the nanocrystal is not the same as the pressure applied from the outside. A simple model which describes this effect is given in Section 4.

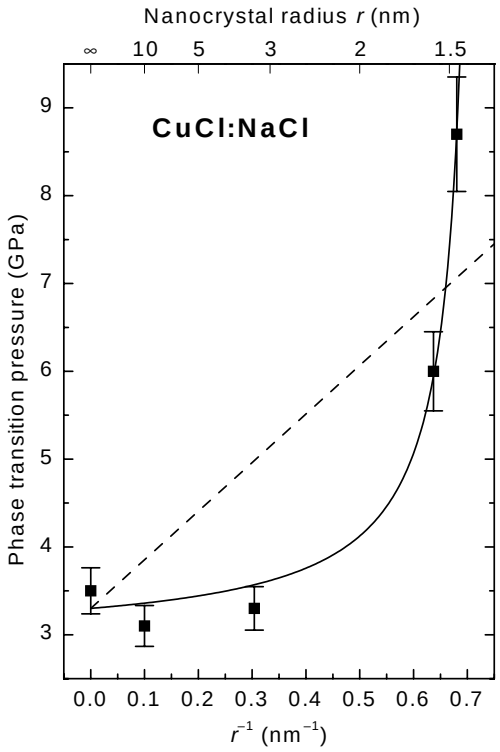

Fig. 7. Size dependence of the phase-transition pressure of CuCl nanocrystals in NaCl from the zinc-blende structure to the first high-pressure phase at a temperature of 7 K. The dashed line is a fit of equation (6) (no surface layer) and the solid line a fit of equation (7) (surface layer of thickness $r_{\rm s}$).

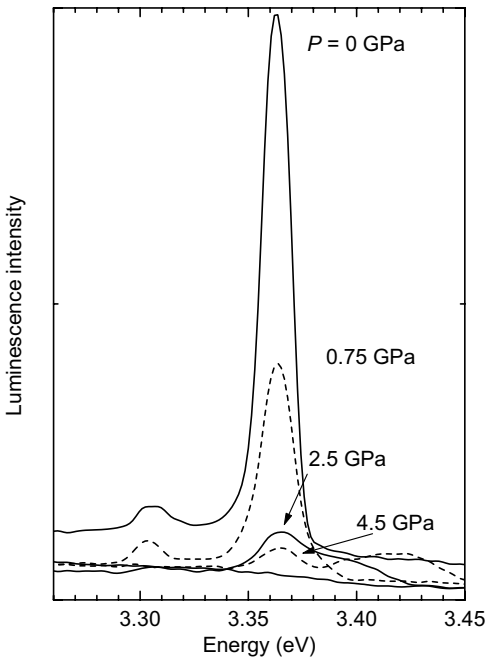

Fig. 8. Luminescence spectra of CuCl nanocrystals in KCl at $T = 7$ K.

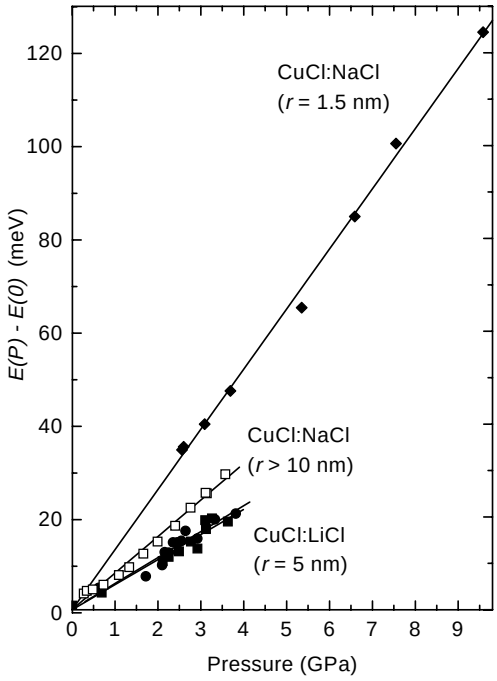

Fig. 9. Exciton energy shifts *versus* pressure for CuCl nanocrystals in NaCl and in LiCl at $T = 7$ K. The lines are linear fits.

3.1.3 CuCl nanocrystals in KCl

In the case of CuCl nanocrystals in KCl the matrix itself shows a structural phase transition from the sodium-chloride to the cesium-chloride structure [28]. At room temperature this phase transition occurs at about 2 GPa. At lower temperatures one expects the phase-transition at a lower pressure. In any case, the phase transition in bulk KCl occurs at a lower pressure than the phase transition in bulk CuCl.

Luminescence spectra of CuCl nanocrystals in KCl for different pressures are shown in Figure 8. The decrease of the zinc-blende luminescence from CuCl takes place at much lower pressures than in the other matrices. One obtains a phase-transition pressure of 0.5 GPa, which means that the phase transitions in both CuCl and KCl occur simultaneously. This indicates a strong interaction between the matrix and the nanocrystal, which is not surprising since the sublattice of the chlorine atoms is the same for both materials.

3.2 Pressure coefficients of exciton energies in CuCl nanocrystals

In a previous publication [29] we had determined the pressure shift of the Z_3 exciton for CuCl nanocrystals in LiCl. It was found that the pressure coefficient for LiCl (5.5 meV/GPa) is considerably smaller than for bulk CuCl (7.65 meV/GPa) [27].

In the course of the present work we have measured the shift of the Z_3 exciton for nanocrystals in NaCl. All results are shown in Figure 9. Samples with small nanocrystals ($T_{\rm gr} = 320$ K and $T_{\rm gr} = 300$ K) show rather high linear pressure coefficients of 12.0 ± 0.5 meV/GPa. In contrast, the pressure coefficient obtained for large nanocrystals (7.9 ± 0.3 meV/GPa) is (within experimental error) equal to the one for bulk CuCl.

4 Discussion

4.1 Influence of the surface energy on phase transitions

We will now briefly discuss the influence of the surface energy on the equilibrium conditions for phase transitions. In the case of isotropic phases this was done for the first time by Gibbs, Thomson, and Laplace (see, *e.g.*, [34]). For simplicity we assume spherical nanocrystals in the following calculations. There are indications that CuCl nanocrystals may have cubic shapes [30,31], but since the calculation depends only on the ratio of surface area and volume, any other shape results in essentially the same equations with perhaps different numerical factors. This is even true if the surface tension depends on the orientation of the surface.

The break of symmetry at the pressure-induced phase transition is of less importance because a hydrostatic pressure probes mainly the change of volume $\Delta V/V$. Although the change of symmetry is controversially discussed for this phase transition [32,33] all authors agree that noncubic distortions are smaller than $\Delta V/V$.

Two phases 1 and 2 can coexist in equilibrium if their chemical potentials μ_i are equal. The chemical potential can be calculated as the first derivative of the Gibbs free energy G with respect to the particle number N. For small particles one has to include in G the surface energy F_A. In the general case F_A is given by $F_A = \sum_i \gamma_i A_i$. The sum extends over all possible orientations of surface areas A_i with the corresponding surface tensions γ_i. If we consider geometrically similar particles, the ratios A_i/A are independent of size. Therefore F_A can be expressed as $F_A = \gamma A$ with γ an average surface tension and A the total surface area. Thus the total Gibbs free energy is equal to

$$G = Nf + PNv + F_A, \tag{2}$$

with the free energy per molecule f and the molecular volume v. This results in the following expression for the chemical potential for a spherical particle with radius r:

$$\mu = f + Pv + \frac{\partial \gamma A}{\partial N} = f + Pv + \frac{2v\gamma}{r}, \tag{3}$$

with $A = 4\pi r^2$ and $Nv = \frac{4\pi}{3} r^3$. The pressure P_∞ for the transition from phase 1 to phase 2 for bulk material ($r = \infty$) can be found from

$$f_1 + P_\infty v_1 = f_2 + P_\infty v_2. \tag{4}$$

It is equal to:

$$P_\infty = \frac{f_2 - f_1}{v_1 - v_2}\,. \tag{5}$$

Analogous, the phase transition pressure P_r for particles with radius r_1 (in phase 1) is given by:

$$\begin{aligned} P_r &= \frac{f_2 - f_1 + \frac{2\gamma_2 v_2}{r_2} - \frac{2\gamma_1 v_1}{r_1}}{v_1 - v_2} \\ &= P_\infty + \left[\frac{2v_1^{1/3}}{v_1 - v_2} \left(\gamma_2 v_2^{2/3} - \gamma_1 v_1^{2/3} \right) \right] \frac{1}{r_1} \\ &= P_\infty + \gamma_{\text{eff}} \frac{1}{r_1}. \end{aligned} \tag{6}$$

Since the square brackets contain only material parameters, we have introduced an effective surface tension γ_{eff}. Depending on the sign of γ_{eff}, P_T either increases or decreases with decreasing nanocrystal size. Whereas $v_1 - v_2$ is always positive for a pressure-induced phase transition (assuming phase 2 to be the high-pressure phase), the sign of the term in parentheses in equation (6) is not known *a priori*. There exist examples both for negative [35,36] and positive [37] signs of γ_{eff}. Since we had found an increase of P_T for small nanocrystals, γ_{eff} has to be positive for CuCl nanocrystals in NaCl.

The dashed line in Figure 7 show the best fit of equation (6) to our data (the value of P_∞ was held fixed at 3.3 GPa). Whereas the trend is correct, the values are well outside the experimental errors. One possible reason for the failure of equation (6) is the assumption that the surface is infinitely thin (at least thin compared to the particle size). This assumption can obviously not be true for nanocrystals with a radius of, *e.g.*, 1.5 nm, which is less than three lattice constants. The simplest way to include a finite thickness of the surface is to replace r_1 in equation (6) by $r_1 - r_{\text{s}}$ which yields

$$P_r = P_\infty + \gamma_{\text{eff}} \frac{1}{r_1 - r_{\text{s}}}, \tag{7}$$

where we have introduced a surface layer with thickness r_{s}. A fit of equation (7) results in the solid line in Figure 7, which obviously fits the experimental results very well. The parameters obtained from the fit are $\gamma_{\text{eff}} = 0.5 \pm 0.1$ J/m^2 and $r_{\text{s}} = 1.37 \pm 0.02$ nm. Since these parameters have not been determined for the system CuCl:NaCl before, it is not possible to compare them with other results. The order of magnitude for γ_{eff} is the same as, *e.g.*, for CdS and CdSe. In these materials values between 0.2 and 0.4 J/m^2 have been determined [4–6]. For two reasons we believe that the observed thickness of the surface layer is reasonable although for small nanocrystals the volume of the surface layer may exceed the volume of the nanocrystal core. First of all typical theoretical calculations [38] show that the influence of the surface extends to a depth of about four monolayers (our value for r_{s} is equal to about five monolayers or 2.5 lattice constants of CuCl). Furthermore, the elastic interaction between CuCl nanocrystals and the NaCl matrix, which was demonstrated by elastic measurements [39] supports the development of the surface layer.

In contrast to the first pressure-induced phase transition in CuCl nanocrystals, which is size dependent, the second phase transition to the sodium-chloride phase is independent of the nanocrystal size. There are two possible explanations for this: 1. The effective surface tension is very small. 2. The nanocrystals do not undergo the first phase transition as a whole, so that one zinc-blende nanocrystal becomes a number of smaller nanocrystals in the high-pressure phase. This could mean that after this phase transition all nanocrystals have about the same size. Accordingly the second phase transition occurs at the same pressure independent of the initial size. This can also explain the rather high value of 15 GPa for this phase transition compared to 10 GPa for bulk CuCl [14].

4.2 Pressure transmission from the matrix to the nanocrystals

Comparing LiCl and NaCl as matrices, we found a smaller pressure coefficient and a higher phase transition pressure for LiCl. Both effects can be explained if one assumes that the pressure acting on the nanocrystals is different from the pressure applied from outside. If this assumption is true the ratio of the pressure coefficients in both matrices must be equal to the inverse ratio of the phase-transition pressures:

$$\frac{\mathrm{d}E/\mathrm{d}P(\text{NaCl})}{\mathrm{d}E/\mathrm{d}P(\text{LiCl})} = \frac{P_T(\text{LiCl})}{P_T(\text{NaCl})}\,. \tag{8}$$

Our experimental results yield 1.4 on the left-hand side and 1.3 on the right-hand side. Within experimental error these two values agree. This result has motivated us to develop a simple model for the elastic interaction between the nanocrystals and the matrix.

The assumption made above can be further justified by a simple model. We consider both nanocrystal and matrix as isotropic elastic continua. The nanocrystal is a sphere with radius r_i in an infinite matrix. The system is subject to a hydrostatic pressure P. In this case only a radial displacement component ϵ_r occurs. Using polar coordinates only the following components of the stress tensor T and of the strain tensor S exist:

$$T_{rr} = -P(r), \quad S_{rr} = \frac{\partial \epsilon_r}{\partial r}, \quad S_{\theta\theta} = \frac{\epsilon_r}{r}, \quad S_{\varphi\varphi} = \frac{\epsilon_r}{r}\,. \tag{9}$$

At the interface between nanocrystal and matrix $S_{\theta\theta}$ and $S_{\varphi\varphi}$ have to be continuous. From these boundary conditions at $r = r_i$ the pressure P_{NC} at the nanocrystal is given by [40]:

$$P_{\text{NC}} = \frac{9B(1-\nu)}{2Y + 3(1+\nu)B} P. \tag{10}$$

In this equation B is the bulk modulus of the nanocrystal material, Y Young's modulus of the matrix and ν Poisson's ratio of the matrix.

Using the elastic constants of NaCl and LiCl, we find from equation (10) that P_{NC} in NaCl is 1.33 times larger

than in LiCl. This value coincides well with our experimentally determined ratios of 1.3 and 1.4 (see above).

One should note that P_{NC} in equation (10) does not depend on the nanocrystal radius. Thus the size dependence of the phase-transition pressure of CuCl nanocrystals in NaCl cannot be explained by this effect.

4.3 Size dependence of the exciton pressure coefficients

We had found a considerably larger pressure coefficient for small nanocrystals (12 meV/GPa for $r = 1.5$ nm) than for large nanocrystals (7.9 meV/GPa for $r > 10$ nm) or bulk. For an explanation we have to consider the influence of the confinement on the pressure dependence of the exciton energy. The pressure dependence of the exciton energy in nanocrystals consists of the following terms:

$$\frac{\mathrm{d}E}{\mathrm{d}P} = \left.\frac{\mathrm{d}E}{\mathrm{d}P}\right|_{\mathrm{bulk}} + \left.\frac{\mathrm{d}E}{\mathrm{d}P}\right|_{\mathrm{size}} + \left.\frac{\mathrm{d}E}{\mathrm{d}P}\right|_{\mathrm{mass}}. \qquad (11)$$

The first term is equal to the bulk effect. Apart from the bulk pressure dependence there are two terms which describe the change of the confinement energy under pressure. $\mathrm{d}E/\mathrm{d}P|_{\mathrm{size}}$ is due to the decrease of the nanocrystal size and $\mathrm{d}E/\mathrm{d}P|_{\mathrm{mass}}$ is due to the change in exciton mass under pressure. According to equation (1) both effects change the confinement energy.

Using Murnaghan's law [41] for the dependence of volume on pressure:

$$V(P) = V_0 \left(1 + \frac{B'}{B} P\right)^{-\frac{1}{B'}}, \qquad (12)$$

we obtain for nanocrystals with a size of $r = 1.5$ nm for $\mathrm{d}E/\mathrm{d}P|_{\mathrm{size}}$ a value of 0.8 meV/GPa.

The pressure dependence of the exciton mass M is estimated from the pressure dependence of the gap energy E_{g} by $\boldsymbol{k} \cdot \boldsymbol{p}$ perturbation theory [42–44]:

$$\begin{aligned} M &= m_e + m_h, \\ \frac{m_0}{m_e} &= 1 + 2\frac{X^2}{m_0 E_{\mathrm{g}}}, \\ \frac{m_0}{m_h} &= 1 - \frac{2}{3}\frac{X^2}{m_0 E_{\mathrm{g}}}. \end{aligned} \qquad (13)$$

m_e and m_h are electron and hole masses, m_0 is the free electron mass, and X is the momentum matrix element between valence and conduction bands, which can be assumed to be pressure-independent. Inserting experimental data ($\mathrm{d}E_{\mathrm{g}}/\mathrm{d}P = 4.1$ meV/GPa [27] and $M = 2.3\ m_0$ [45]) we find from equation (13) a decrease of the total exciton mass at a rate of $-0.002\ m_0$/GPa. This results, again for nanocrystals with $r = 1.5$ nm, in a value for $\mathrm{d}E/\mathrm{d}P|_{\mathrm{mass}}$ of 0.2 meV/GPa.

Adding the contributions of equations (12) and (13), the confinement energy increases with pressure at a rate of 1 meV/GPa. This is about one fourth of the difference in pressure coefficients between small (12 meV/GPa) and large (7.9 meV/GPa) nanocrystals. An additional effect stems from the size distribution of the nanocrystals. Because of the size dependence of the phase transition large nanocrystals undergo their phase transition at lower pressures. The remaining signal comes only from the nanocrystals still in the zinc-blende phase. Thus their average size decreases with pressure, which leads to a higher apparent pressure coefficient.

5 Conclusions

We have found a strong increase of the phase-transition pressure P_T for small CuCl nanocrystals in NaCl, which is caused by the contribution of the elastic interaction at the surface between nanocrystal and matrix. As shown by a comparison between NaCl and LiCl matrices, the pressure acting on the nanocrystal is not necessarily the same as the pressure applied from outside. The phase transition of CuCl nanocrystals in KCl occurs simultaneously with the phase transition in KCl. This again demonstrates the important role of the elastic interaction between nanocrystals and matrix.

This work was supported by the Deutsche Forschungsgemeinschaft. We gratefully acknowledge the donation of material for the diamond anvil cell by Krupp VDM GmbH, Werdohl.

References

1. *Proceedings of the 22nd International Conference on the Physics of Semiconductors, Vancouver 1994*, edited by D.J. Lockwood (World Scientific, Singapore, 1995).
2. *Proceedings of the 23nd International Conference on the Physics of Semiconductors, Berlin 1996*, edited by M. Scheffler, R. Zimmermann (World Scientific, Singapore, 1996).
3. *Proceedings of the 24th International Conference on the Physics of Semiconductors, Jerusalem 1998*, edited by D. Gershoni (World Scientific, Singapore, 1999).
4. S.H. Tolbert, A.P. Alivisatos, Science **265**, 373 (1994).
5. M.R. Silvestri, J. Schroeder, J. Phys.-Cond. **7**, 8519 (1995).
6. J. Schroeder, P.D. Persans, J. Lumin. **70**, 69 (1996).
7. R. Defay, I. Prigogine, A. Bellemans, D.H. Everett, *Surface Tension and Adsorption* (Longmans, London, 1966).
8. D. Fröhlich, M. Haselhoff, K. Reimann, T. Itoh, Solid St. Commun. **94**, 189 (1995).
9. M. Haselhoff, H.-J. Weber, Phys. Rev. B **58**, 5052 (1998).
10. V. Meisalo, M. Kalliomäki, High Temp.–High Pressures **5**, 663 (1973).
11. A.P. Rusakov, S.G. Grigoryan, A.V. Omel'chenko, A.E. Kadyshevich, Zh. Eksp. Teor. Fiz. **72**, 726 (1977) [Sov. Phys. JETP **45**, 380 (1977)].
12. H. Müller, S. Ves, H.D. Hochheimer, M. Cardona, A. Jayaraman, Phys. Rev. B **22**, 1052 (1980).
13. G.J. Piermarini, F.A. Mauer, S. Block, A. Jayaraman, T.H. Geballe, G.W. Hull, Jr., in *High Pressure Science and Technology*, edited by B. Vodar, P. Marteau (Pergamon, Oxford, 1980), Vol. 1, p. 395.

14. S. Ves, D. Glötzel, M. Cardona, H. Overhof, Phys. Rev. B **24**, 3073 (1981).
15. S. Hull, D.A. Keen, Phys. Rev. B **50**, 5868 (1994).
16. H.-C. Hsueh, J.R. Maclean, G.Y. Guo, M.-H. Lee, S.J. Clark, G.J. Ackland, J. Crain, Phys. Rev. B **51**, 12216 (1995).
17. M. Haselhoff, H.-J. Weber, Mater. Res. Bull. **30**, 607 (1995).
18. Al.L. Éfros, A.L. Éfros, Fiz. Tekh. Poluprovodn **16**, 1209 (1982) [Sov. Phys. Semicond. **16**, 772].
19. T. Itoh, Y. Iwabuchi, M. Kataoka, Phys. Status Solidi B **145**, 567 (1988).
20. G. Huber, K. Syassen, W.B. Holzapfel, Phys. Rev. B **15**, 5123 (1977).
21. G.J. Piermarini, S. Block, J.D. Barnett, R.A. Forman, J. Appl. Phys. **46**, 2774 (1975).
22. H.K. Mao, P.M. Bell, J.W. Shaner, D.J. Steinberg, J. Appl. Phys. **49**, 3276 (1978).
23. W.L. Vos, M.G.E. van Hinsberg, J.A. Schouten, Phys. Rev. B **42**, 6106 (1990).
24. K. Reimann, High Pressure Res. **15**, 73 (1996).
25. J. Thomasson, Y. Dumont, J.-C. Griveau, C. Ayache, Rev. Sci. Instrum. **68**, 1514 (1997).
26. K.S. Song, R.T. Williams, *Self-Trapped Excitons*, 2nd edn. (Springer, Berlin, 1996).
27. K. Reimann, St. Rübenacke, Phys. Rev. B **49**, 11021 (1994).
28. *Landolt-Börnstein – Zahlenwerte und Funktionen aus Naturwissenschaft und Technik*, edited by K.-H. Hellwege, A.M. Hellwege (Springer, Berlin, 1973), Vol. III/7a.
29. K. Reimann, M. Haselhoff, St. R'benacke, M. Steube, Phys. Status Solidi B **198**, 71 (1996).
30. T. Itoh, S. Yano, N. Katagiri, Y. Iwabuchi, C. Gourdon, A.I. Ekimov, J. Lumin. **60-61**, 396 (1994).
31. N. Sakakura, Y. Masumoto, Phys. Rev. B **56**, 4051 (1997).
32. A. Blacha, N.E. Christensen, M. Cardona, Phys. Rev. B **33**, 2413 (1986).
33. D.C. Hutchings, B.S. Wherrett, Phys. Rev. B **50**, 4622 (1994).
34. *Nucleation*, edited by A.C. Zettlemoyer (Dekker, New York, 1969).
35. H. Saka, Y. Nishikawa, T. Imura, Philos. Mag. A **57**, 895 (1988).
36. A.L. Kartuzhanskii, L.K. Kudryashov, V.A. Reznikov, O.I. Smirnova, G.I. Tsereteli, Opt. Spectrosc. (USSR) **69**, 784 (1991).
37. M. Haase, A.P. Alivisatos, J. Phys. Chem. **96**, 6756 (1992).
38. M. Said, F. Máca, K. Kambe, M. Scheffler, N.E. Christensen, Phys. Rev. B **38**, 8505 (1988).
39. H.-J. Weber, K. Lüghausen, M. Haselhoff, H. Siegert, Phys. Status Solidi B **191**, 105 (1995).
40. L.D. Landau, E.M. Lifschitz, *Lehrbuch der Theoretischen Physik VII û Elastizitätstheorie*, 6th edn. (Akademie-Verlag, Berlin, 1989).
41. F.D. Murnaghan, Proc. Nat. Acad. Sci. USA **44**, 244 (1944).
42. E.O. Kane, in *Semiconductors and Semimetals*, edited by R.K. Willardson, A.C. Beer (Academic Press, New York, 1966), Vol. 1, p. 75.
43. E.O. Kane, J. Phys. Chem. Solids **1**, 249 (1957).
44. P.Y. Yu, M. Cardona, *Fundamentals of Semiconductors* (Springer, Berlin, 1996).
45. T. Takagahara, Phys. Rev. B **39**, 10206 (1989).